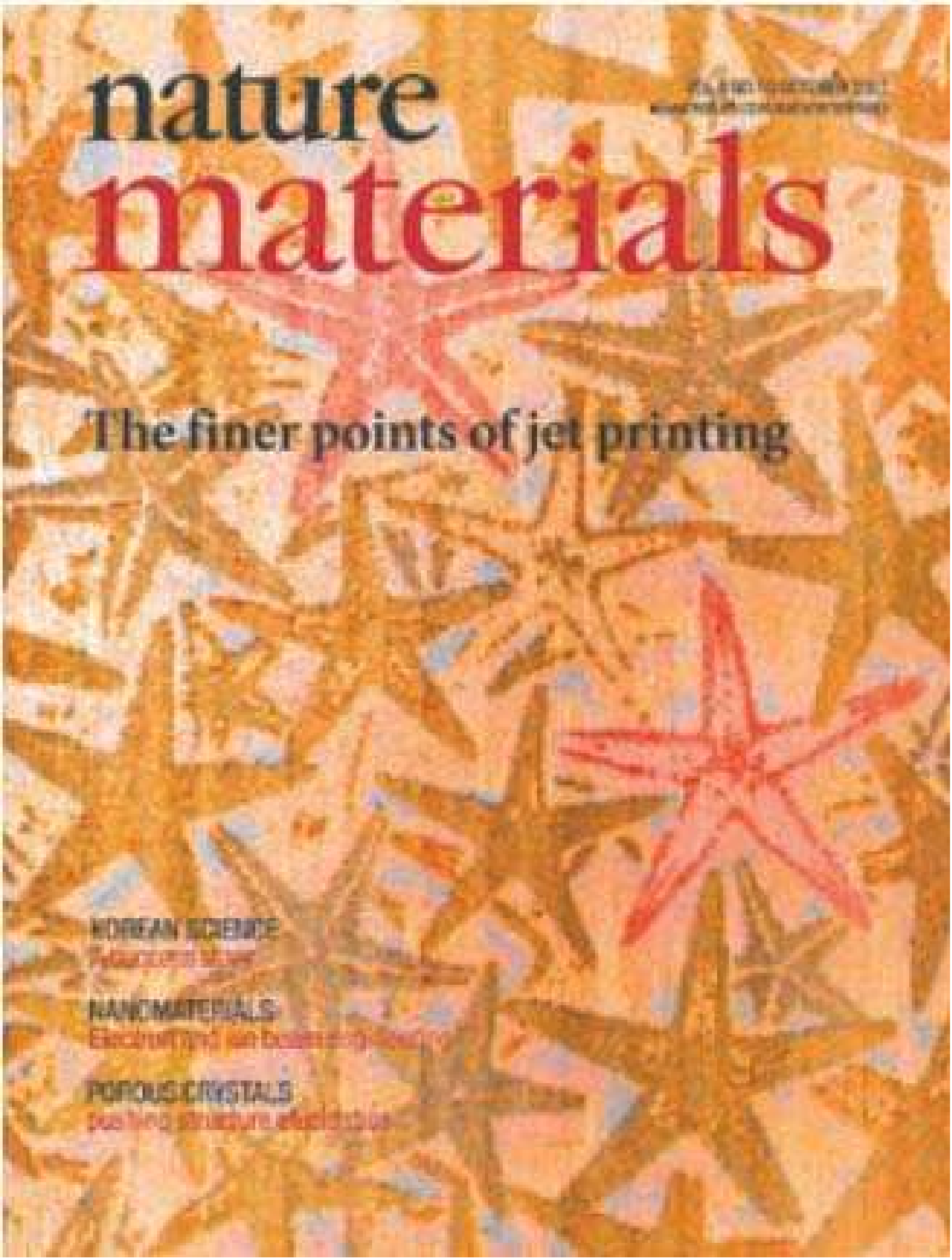
nature
materials
The finer points of jet printing

# High-resolution electrohydrodynamic jet printing

JANG-UNG PARK[1], MATT HARDY[1], SEONG JUN KANG[1,2], KIRA BARTON[3], KURT ADAIR[3], DEEP KISHORE MUKHOPADHYAY[3], CHANG YOUNG LEE[4], MICHAEL S. STRANO[4], ANDREW G. ALLEYNE[3], JOHN G. GEORGIADIS[3], PLACID M. FERREIRA[3] AND JOHN A. ROGERS[1,3]*

[1]Department of Materials Science and Engineering, Beckman Institute, and Frederick Seitz Materials Research Laboratory, University of Illinois at Urbana-Champaign, 1304 West Green Street, Urbana, Illinois 61801, USA

[2]Division of Advanced Technology, Korea Research Institute of Standards and Science, 1 Doryong-Dong, Yuseong-Gu, Daejon 305-340, South Korea

[3]Department of Mechanical Science and Engineering, University of Illinois at Urbana-Champaign, Urbana, Illinois 61801, USA

[4]Department of Chemical & Biomolecular Engineering, and Beckman Institute, University of Illinois at Urbana-Champaign, Urbana, Illinois 61801, USA

*e-mail: jrogers@uiuc.edu

Published online: 5 August 2007; doi:10.1038/nmat1974

**Efforts to adapt and extend graphic arts printing techniques for demanding device applications in electronics, biotechnology and microelectromechanical systems have grown rapidly in recent years. Here, we describe the use of electrohydrodynamically induced fluid flows through fine microcapillary nozzles for jet printing of patterns and functional devices with submicrometre resolution. Key aspects of the physics of this approach, which has some features in common with related but comparatively low-resolution techniques for graphic arts, are revealed through direct high-speed imaging of the droplet formation processes. Printing of complex patterns of inks, ranging from insulating and conducting polymers, to solution suspensions of silicon nanoparticles and rods, to single-walled carbon nanotubes, using integrated computer-controlled printer systems illustrates some of the capabilities. High-resolution printed metal interconnects, electrodes and probing pads for representative circuit patterns and functional transistors with critical dimensions as small as 1 μm demonstrate potential applications in printed electronics.**

Printing approaches used in the graphic arts, particularly those based on ink-jet techniques, are of interest for applications in high-resolution manufacturing owing to attractive features that include (1) the possibility for purely additive operation, in which functional inks are deposited only where they are needed, (2) the ability to pattern directly classes of materials such as fragile organics or biological materials that are incompatible with established patterning methods such as photolithography, (3) the flexibility in choice of structure designs, where changes can be made rapidly through software-based printer-control systems, (4) compatibility with large-area substrates and (5) the potential for low-cost operation[1–3]. Conventional devices for ink-jet printing rely on thermal or acoustic formation and ejection of liquid droplets through nozzle apertures[3]. A growing number of reports describe adaptations of these devices with specialized materials in ink formats for applications in electronics[4–9], information display[10–12], drug discovery[13,14], micromechanical devices[15,16] and other areas[3,17]. The functional resolution in these applications, as defined by the narrowest continuous lines or smallest gaps that can be created reliably, is ~20–30 μm (refs 9,18–20). This coarse resolution results from the combined effects of droplet diameters that are usually no smaller than ~10–20 μm (2–10 pl volumes) and placement errors that are typically ±10 μm at standoff distances of ~1 mm (refs 5,21,22). Some methods can avoid these limitations, for certain classes of features. For example, lithographically predefined assist features[5,23,24] or surface functionalization of pre-printed inks[25] in the form of patterns of wettability or surface relief can confine and guide the flow of the droplets as they land on the substrate. In this manner, gaps between printed droplets, for example, can be controlled at the submicrometre level[23–25]. This capability is important for applications in electronics when such gaps define transistor channel lengths. These methods do not, however, offer a general approach to high resolution. In addition, they require separate patterning systems and processing steps to define the assist features.

Electrohydrodynamic jet (e-jet) printing is a technique that uses electric fields, rather than thermal or acoustic energy, to create the fluid flows necessary for delivering inks to a substrate. This approach has been explored for modest-resolution applications (dot diameters $\geq$20 μm using nozzle diameters $\geq$50 μm) in the graphic arts[26–29]. To our knowledge, it is unexamined for its potential to provide high-resolution (that is, $<$10 μm) patterning or to fabricate devices in electronics or other areas of technology by use of functional or sacrificial inks. Here, we introduce methods and materials for e-jet printing with resolution well within the submicrometre range. Patterning of wide ranging classes of inks in diverse geometries illustrates some of the capabilities. Printed electrodes for functional transistors and representative circuit designs demonstrate potential applications in electronics. These results define some advantages and disadvantages of this approach, in its current form, compared with other ink printing techniques.

Figure 1 shows a schematic diagram of our e-jet printing system. A syringe pump (flow rates $\leq$ ~30 pl $s^{-1}$) or pneumatic pressure controller (applied pressure $\leq$ ~5 psi) connected to a

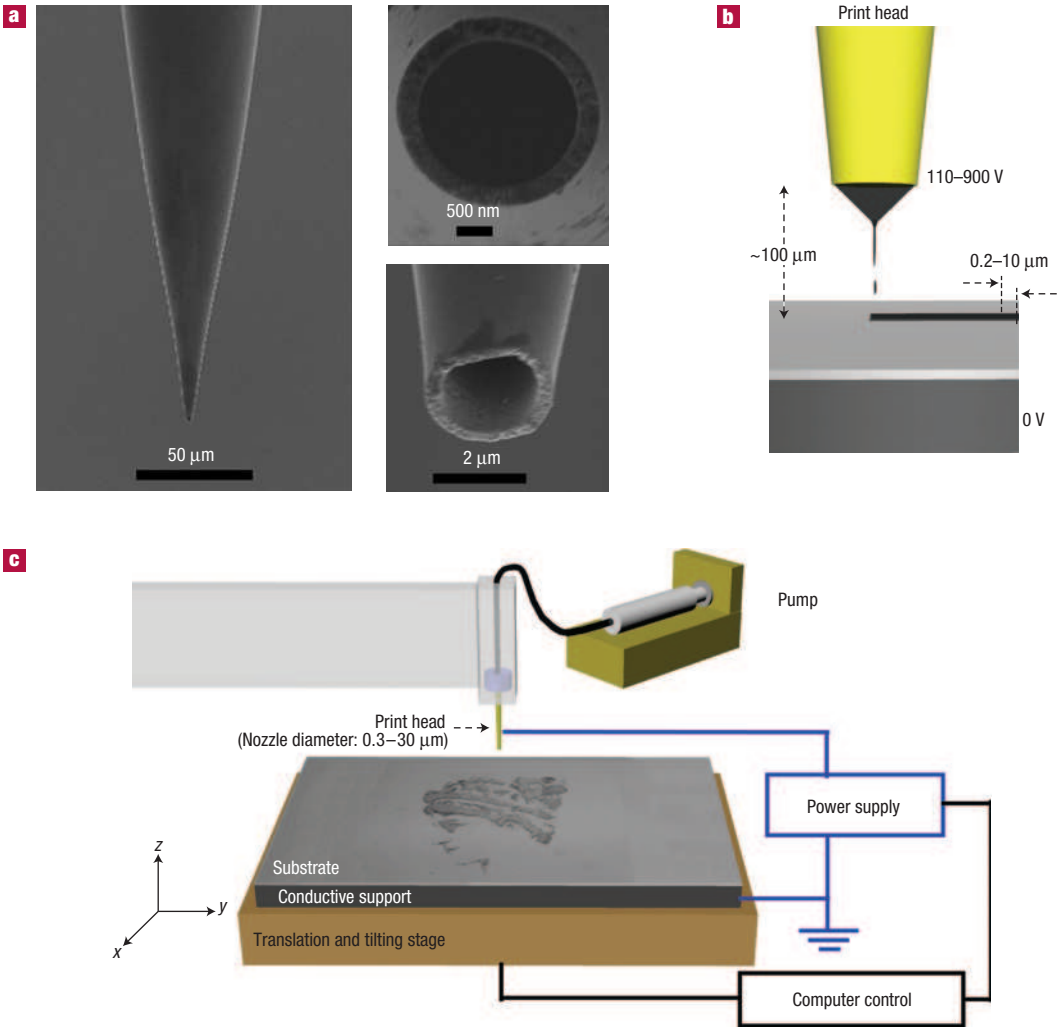


**Figure 1 Nozzle structures and schematic diagrams of a high-resolution e-jet printer. a**, SEM images of a gold-coated glass microcapillary nozzle (2 μm internal diameter). A thin film of surface-functionalized Au coats the entire outer surface of the nozzle as well as the interior near the tip. The insets on the right show views of this tip region. **b**, Nozzle and substrate configuration for printing. Ink ejects from the apex of the conical ink meniscus that forms at the tip of the nozzle owing to the action of a voltage applied between the tip and ink, and the underlying substrate. These droplets eject onto a moving substrate to produce printed patterns. In this diagram, the substrate motion is to the right. Printed lines with widths as small as 700 nm can be achieved in this fashion. **c**, Printer set-up. A gold-coated nozzle (internal diameter: 1, 2 or 30 μm) is located above a substrate that rests on a grounded electrode with a separation (H) of ~100 μm. A power supply connects to the nozzle and the electrode under the substrate. The substrate/electrode combination mounts on a five-axis (*x*, *y*, *z* axes and two tilting axes in the *x*–*y* plane) stage for printing.

glass capillary (internal diameter of between 0.3 and 30 μm and outer diameter of between 0.5 and 45 μm) delivers fluid inks to the cleaved end of the capillary, which serves as a nozzle. The nozzle fabrication process is described in the Methods section. Figure 1a shows scanning electron microscope (SEM) images of the nozzle and the nozzle opening. A thin film of sputter-deposited gold coats the entire outside of the microcapillary as well as the area around the nozzle and the inner surfaces near the tip. A hydrophobic self-assembled monolayer (1H,1H,2H,2H-perfluorodecane-1-thiol) formed on the gold limits the extent to which the inks wet the regions near the nozzle, thereby minimizing the probability for clogging and/or erratic printing behaviour (see Supplementary Information, Table S1). We refer to this functionalized gold-coated capillary mounted on a mechanical support fixture and connected to the pump as the e-jet print head. The nozzles used in these print heads have internal diameters that are much smaller than those used in previous work on e-jet printing[26–29], where the focus was on relatively low-resolution applications in graphic arts. The small nozzle dimensions are critically important to achieving high-resolution performance for device fabrication, for reasons described below.

A voltage applied between the nozzle and a conducting support substrate creates electrohydrodynamic phenomena that drive flow of fluid inks out of the nozzle and onto a target substrate. This substrate rests on a metal plate that provides an electrically grounded conducting support. The plate, in turn, rests on a plastic vacuum chuck that connects to a computer-controlled $x, y$ and $z$ axes translation stage. A two-axis tilting mount on top of the translation stage provides adjustments to ensure that motion in the $x$ and $y$ directions does not change the separation ($H$, typically ~100 μm) between the nozzle tip and the target substrate. A d.c. voltage ($V$) applied between the nozzle and the metal plate with

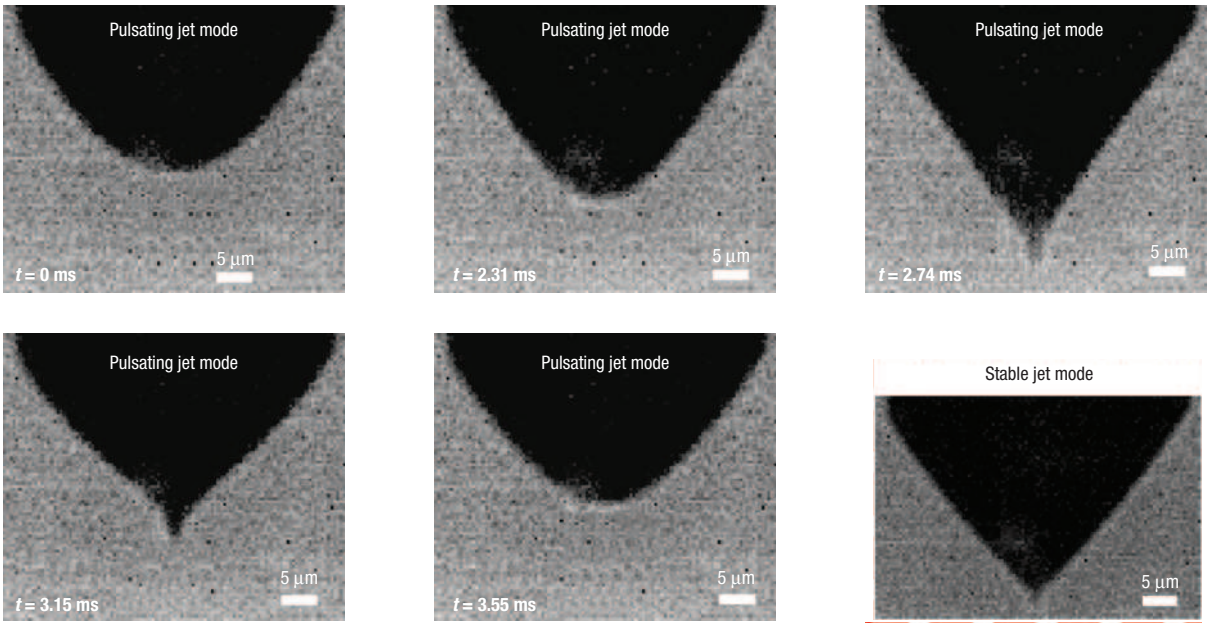


**Figure 2 Time-lapse images of the pulsating liquid meniscus in one cycle at $V/H = 3.5\,V\,\mu m^{-1}$.** $V$ is the applied voltage between the nozzle and the substrate and $H$ is the distance between the nozzle tip and the substrate. The bottom right image corresponds to the stable jet mode, which is achieved at $V/H \sim 9\,V\,\mu m^{-1}$ for this system. These images were captured at a frame rate of 66,000 fps and exposure time of 11 μs, using a high-speed camera. The reference time ($t = 0$) corresponds to the time at which the meniscus first reaches its fully retracted state.

a computer-controlled power supply generates an electric field that causes mobile ions in the ink to accumulate near the surface of the pendent meniscus at the nozzle. The mutual coulombic repulsion between these ions induces a tangential stress on the liquid surface, thereby deforming the meniscus into a conical shape, known as a Taylor cone[30]. At sufficiently high electric fields, this electrostatic (Maxwell) stress overcomes the capillary tension at the apex of the liquid cone; droplets eject from the apex to expel some portion of the surface charge (Rayleigh limit). Even very small ion concentrations are sufficient to enable this ejection process. For example, in uncontrolled spray modes, ejection is possible with liquids that have electrical conductivities that span ten decades[31], from $10^{-13}$ to $10^{-3}\,S\,m^{-1}$. Coordinating the operation of the power supply with the system of translation stages enables direct-write e-jet printing of inks in arbitrary geometries (see Fig. 1b,c).

To understand the fundamental dynamics of this electric-field-driven jetting behaviour, a high-speed camera (Phantom 630, 66,000 fps) was used to image the process of Taylor-cone deformation and droplet ejection directly at the nozzle. For these experiments, an aqueous ink of a blend of poly(3,4-ethylenedioxythiophene) and poly(styrenesulphonate) (PEDOT/PSS) was used. The images, shown in Fig. 2, show that the meniscus at the nozzle expands and contracts periodically owing to the electric field. A complete cycle, which occurs in roughly 3–10 ms for the systems investigated here, consists of stages of liquid accumulation, cone formation, droplet ejection and relaxation[32]. The initial spherical meniscus at the nozzle tip changes gradually into a conical form owing to the accumulation of surface charges. The radius of curvature at the apex of the cone decreases until the Maxwell stress matches the maximum capillary stress, resulting in charged fluid jet ejection. This ejection decreases the cone volume and charges, thereby reducing the electrostatic stress to values less than the capillary tension. The ejection then stops and the meniscus retracts to its original spherical shape. The apex of the cone can oscillate, leading to the ejection of multiple droplets in short bursts. The frequency of this oscillation, which is in the kHz frequency range, increases in a nonlinear fashion with the electric field[33,34]. After a period of ejection in the form of multiple pulsations similar to the cycle shown in Fig. 2, the retracted spherical meniscus remains stable and largely unperturbed until the next period of ejection. This accumulation time depends on the flow rate imposed by the pump and on the electrical charging times associated with the resistance and capacitance of the system[33,34].

At sufficiently high fields, a stable jet mode (as opposed to the pulsating mode described above) can be achieved. In this situation, a continuous stream of liquid emerges from the nozzle, as shown in Fig. 2. At even higher fields, multiple jets can form, culminating ultimately in an atomization mode (e-spray mode) of the type used in mass spectroscopy and other well-established fields of application[35,36]. For controlled high-resolution printing of the type introduced here, this mode must be avoided. Either the stable jet or the pulsating modes can be used. The sensitivity of the stable jet mode to applied fields (too high results in uncontrolled spray, and too low results in pulsation) favours, in a practical sense, the pulsating operation. A key to achieving high resolution, from the standpoint of print-head design, is the use of fine nozzles with sharp tips. Such nozzles lead directly to small droplets/streams. In addition, the low $V$ and $H$ values that result from electric-field-line focusing at the sharp tips of such nozzles and the distribution of the electric field lines themselves combine to minimize lateral variations in the placement of the droplets/streams on the printed substrate (see Supplementary Information, Fig. S1).

A wide range of functional organic and inorganic inks, including suspensions of solid objects, can be printed using this approach, with resolutions extending to the submicrometre range. Figure 3a,b shows dot-matrix text patterns formed using a solution ink of a conducting polymer PEDOT/PSS and a photocurable polyurethane prepolymer (NOA 74, Norland Products) printed

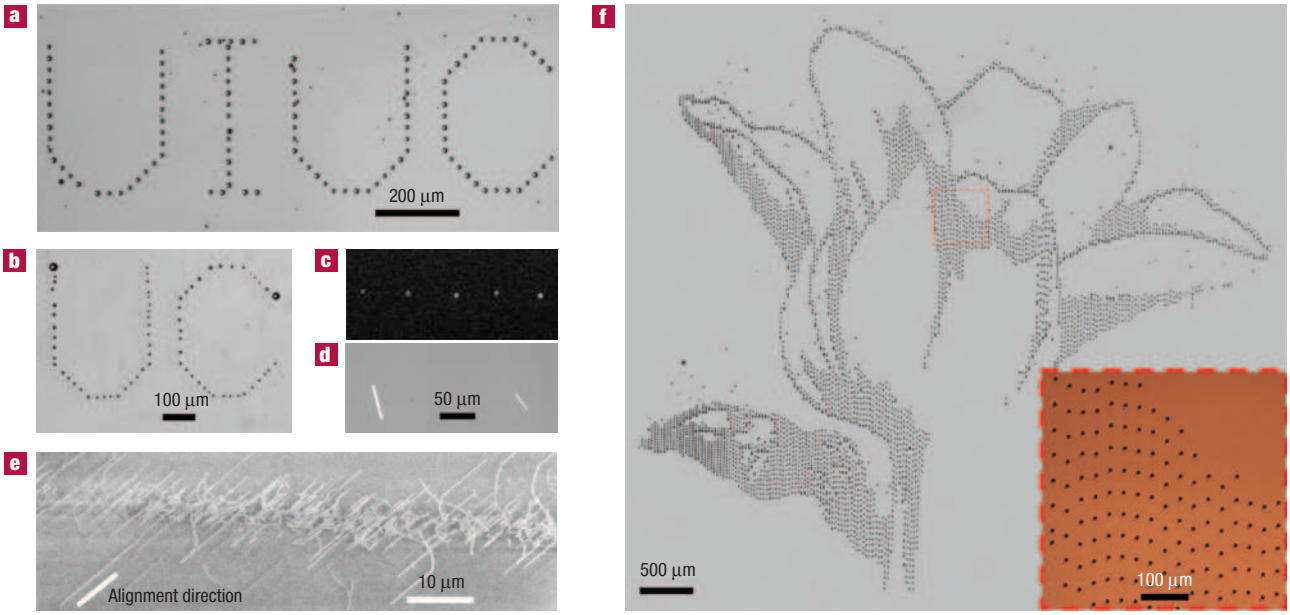


**Figure 3 Optical micrographs and SEM images of various images formed with different inks. a**, Letters printed with the conducting polymer PEDOT/PSS. The average dot diameter is 10 μm. **b**, Letters printed with a photocurable polyurethane polymer with dot diameters of 10 μm. **c**, Fluorescence optical micrograph (emission at 680 nm) of Si nanoparticles (average diameter of 3 nm) printed from a suspension in 1-octanol. The diameter of the printed dots is 4 μm. **d**, Optical micrograph of single-crystal Si rods (thickness: 3 μm, length: 50 μm, width: 2 μm) printed from a suspension in 1-octanol. **e**, SEM image of aligned SWNTs grown by CVD on quartz using printed patterns of ferritin as a catalyst. **f**, Image of a flower formed with printed dots (~8 μm diameters) of SWNTs from an aqueous solution. In all cases, nozzles with internal diameters of 30 μm were used.

onto a $SiO_2$(300 nm)/Si substrate. Figure 3c,d shows examples of printed inks that consist of suspensions of Si nanoparticles (average diameter: 3 nm)[37] and single-crystal Si rods (length: 50 μm, width: 2 μm, thickness: 3 μm)[38] dispersed in 1-octanol. The Si nanoparticles emit fluorescent light at 680 nm wavelength, as shown in Fig. 3c. Suspensions of ferritin nanoparticles can also be printed and then used as catalytic seeds for the chemical vapour deposition (CVD) growth of single-walled carbon nanotubes (SWNTs). Figure 3e shows the results, in which the printing and growth occurred on an annealed ST (stable temperature)-cut quartz substrate[39], to yield well-aligned individual SWNTs. For the structures printed onto $SiO_2$/Si, the silicon formed the conducting support for printing. In the case of quartz, a metal supporting plate was used. Computer-coordinated control of the power supply and the stages enables printing of complex patterns, such as digitized graphic images or circuit layouts. Figure 3f shows a printed image of a flower formed with an ink consisting of surfactant-stabilized SWNTs in water[40]. The average dot diameter is $8 \pm 0.3$ μm, and the uniformity in the sizes is shown in the Supplementary Information, Fig. S2. For the results in Fig. 3, the nozzle internal diameter was 30 μm and the substrates moved at speeds of ~100 μm $s^{-1}$ (1 mm $s^{-1}$ for Fig. 3a,b). These conditions yielded dot-matrix versions of the images with ~10 μm dot diameters. These dots are associated with the accumulation of multiple micro/nanodroplets ejected at the kHz level frequency in the pulsating mode; the separation between these dots corresponds to the accumulation time mentioned previously. (For Fig. 3d, owing to the low concentration of Si rods (~5 rods $nl^{-1}$), a relatively large drop diameter of ~100 μm was selected by applying the voltage for 100 ms with the nozzle held fixed.)

Although the ~10 μm feature sizes shown in Fig. 3 are suitable for various applications, the resolution can be improved by using smaller nozzles. Supplementary Information, Fig. S3 shows a portrait image composed of 2 μm dots printed with a 2-μm-internal-diameter nozzle and a printing speed of 20 μm $s^{-1}$. The printing resolution can be extended much further into the submicrometre regime. Figure 4a shows an image of the ancient scholar, Hypatia, printed using polyurethane ink. Dots ~490 nm in diameter were achieved with a 500-nm-internal-diameter nozzle for this case. Further reducing the internal diameter to 300 nm reduces the dot size to $240 \pm 50$ nm, as shown in Fig. 4b. Patterns of continuous lines and other shapes can be achieved by printing at stage translation speeds that allow the dots to merge. Figure 4c shows patterns of lines printed onto a $SiO_2$/Si substrate using the 2-μm-internal-diameter nozzle and a printing speed of 10 μm $s^{-1}$; the line widths, for single-pass printing, are ~3 μm. With a 1-μm-internal-diameter nozzle, line widths of ~700 nm can be achieved using polyethyleneglycol methyl ether solution (Aldrich), as shown in Fig. 4d. These results represent a resolution that significantly exceeds that of conventional unassisted thermal- or piezoelectric-type ink-jet systems. The slight 'waviness' in the submicrometre dots or lines in Fig. 4a,b,d is due to the combined effects of mechanical resonances in the long capillary used in the print head and slight fluctuations associated with the e-jet process.

Printed electronics represents an important application area that can take advantage of both the extremely high-resolution capabilities of e-jet printing as well as its compatibility with a range of functional inks. To demonstrate the suitability of e-jet printing for fabricating key device elements in printed electronics, we patterned complex electrode geometries for ring oscillators, source/drain electrodes for transistors, and we built working transistors. In these examples, a photocurable polyurethane precursor provided a printable resist layer for patterning metal electrodes by chemical etching. The print head in this case used a

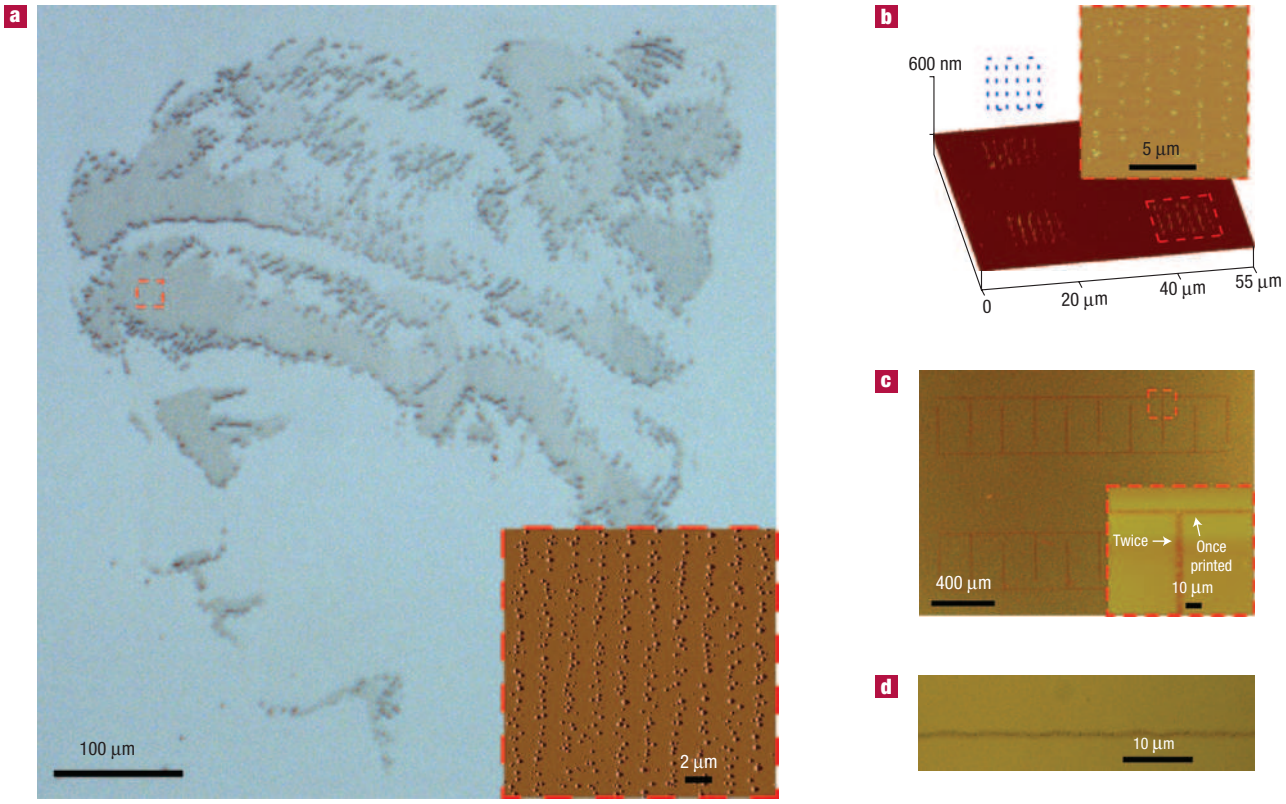


**Figure 4 High-resolution e-jet printing with printed feature sizes in the range from ~240 nm to ~5 μm. a**, Optical micrograph of a portrait of the ancient scholar, Hypatia, printed using a polyurethane ink and a 500-nm-internal-diameter nozzle. The diameters of the dots are ~490 nm. The inset shows an AFM image of the printed dots. **b**, Three-dimensional AFM image of aligned arrays of dots with diameters of 240 ± 50 nm, formed using the polyurethane and a 300-nm-internal-diameter nozzle. The blue dashed lines show the scan direction of the nozzle, and the top right inset shows a magnified AFM image of the printed dot array. **c**, Continuous lines printed using the SWNT ink and a 2-μm-internal-diameter nozzle. The horizontal lines (widths: ~3 μm) were printed in a single pass, whereas the vertical lines (width: ~5 μm) were formed by printing in two passes. **d**, Optical micrograph of a printed line of polyethyleneglycol (width: 700–800 nm) formed using a 1-μm-internal-diameter nozzle.

1-μm-internal-diameter nozzle; the printing speed was 100 μm $s^{-1}$. The substrate consisted of $SiO_2$ (300 nm)/Si coated uniformly with Au (130 nm) and Cr (2 nm). Figure 5a shows a pattern of printed polyurethane after curing by exposure to ultraviolet light (~1 J $cm^{-2}$). The resolution was 2 ± 0.4 μm, as defined by the minimum line widths. Much larger features, shown here in the form of electrode pads with dimensions up to 1 mm, are possible by overlapping the fine lines. Wet etching the printed substrate (Au etchant: trifluoroacetic acid, Transene; Cr etchant: Cr mask etchant, Transene) removed the Au/Cr bilayer in regions not protected by the polyurethane. Removing the polyurethane by soaking in methylene chloride and, in some cases, by oxygen plasma etching (plasmatherm reactive ion etch system, 20 s.c.c.m. $O_2$ flow with a chamber base pressure of 150 mtorr, 150 W, and radiofrequency power for 5 min), completed the fabrication or prepared the substrate for deposition of the next functional material. Figure 5b–e shows various patterns of Au/Cr electrodes formed in this manner. Figure 5d shows an array of printed source/drain electrodes with different spacings (that is, channel lengths, $L$). As shown in the inset of Fig. 5d, channel lengths as small as 1 ± 0.2 μm can be achieved with channel widths of up to hundreds of micrometres (~170 μm in this case). An atomic force microscopy (AFM) image of part of the channel area shows sharp, well-defined edges (Fig. 5e). The ability to print channel lengths with sizes in the micrometre range in a direct fashion, without the use of substrate wetting or relief assist features, is important owing to the key role of this dimension in determining the switching speeds and the output currents of the transistors.

As a demonstration of device fabrication by e-jet printing, thin-film transistors (TFTs) that use perfectly aligned arrays of SWNTs[41] as the semiconductor and e-jet-printed electrodes for source and drain were fabricated on flexible plastic substrates. The fabrication process began with e-beam evaporation of a uniform gate electrode (Cr: 2 nm/Au: 70 nm/Ti: 10 nm) onto a sheet of polyimide (thickness: 25 μm). A layer of $SiO_2$ (thickness: 300 nm) deposited by plasma-enhanced CVD at 250 °C and a spin-cast film of epoxy (SU-8, thickness: 200 nm) formed a bilayer gate dielectric. The epoxy also served as an adhesive for the dry transfer of SWNT arrays grown by CVD on quartz wafers using patterned stripes of iron catalyst[41]. Evaporating uniform layers of Cr (2 nm)/Au (100 nm) onto the transferred SWNT arrays, followed by e-jet printing and photocuring of polyurethane and then etching of the exposed parts of the Cr/Au to define source/drain electrodes completed the fabrication of devices with different channel lengths, $L$. SWNTs outside the channel areas were removed by reactive ion etching (150 mtorr, 20 s.c.c.m. $O_2$, 150 W, 30 s) to isolate these devices. Figure 6a,b shows schematic diagrams of the device layouts and an SEM image of the aligned SWNTs with the e-jet-printed source/drain electrodes. The arrays consist of ~2.5 SWNTs/10 μm. Figure 6c shows typical transfer characteristics that indicate the expected p-channel behaviour[42]. The current outputs increase approximately linearly with $1/L$, with ratios of the 'on' to the 'off'

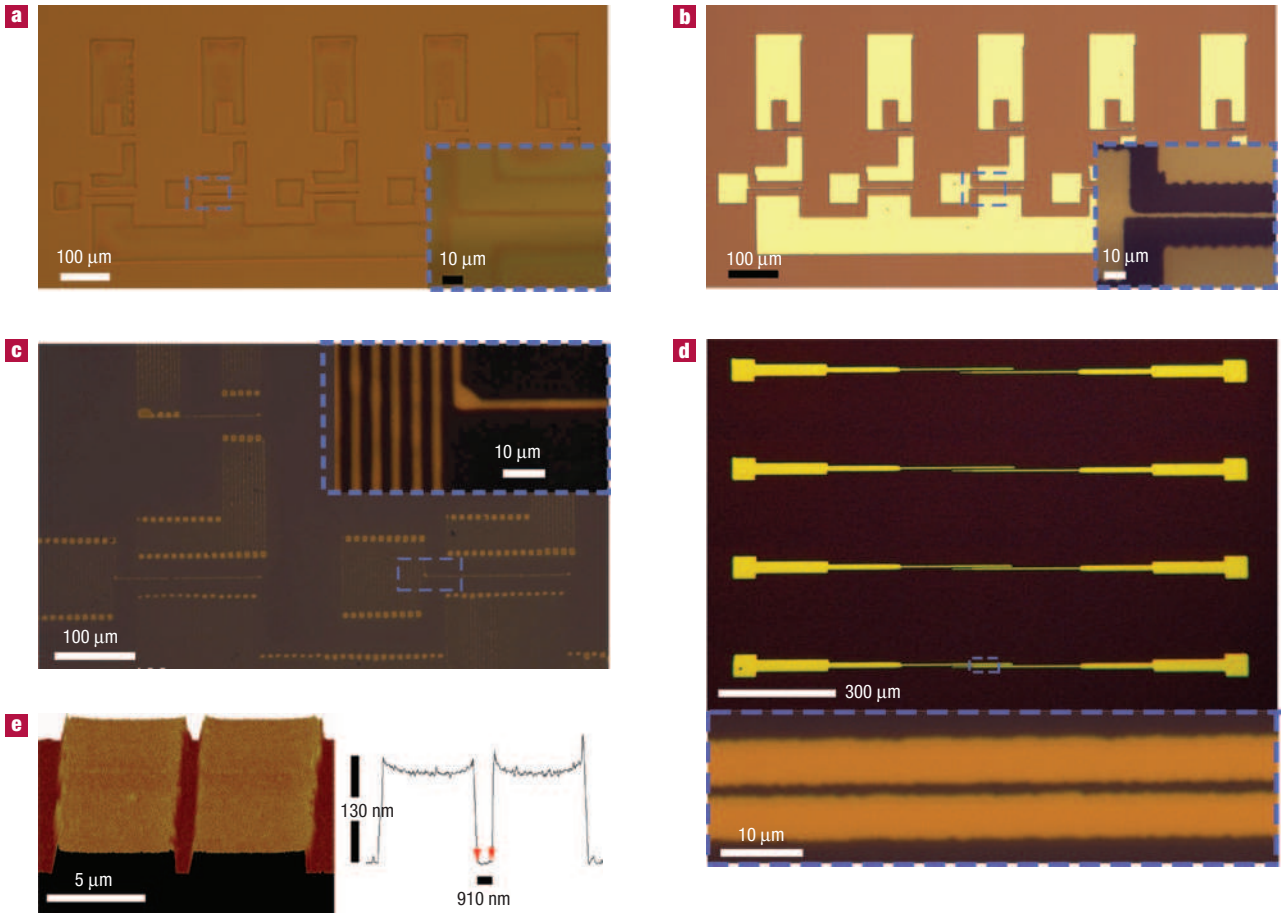


**Figure 5 Patterns of electrode structures for a ring oscillator and isolated transistors formed by e-jet printing of a photocurable polyurethane ink that acts as an etch resist for a uniform underlying layer of metal (Au/Cr). a**, E-jet-printed polyurethane etch resist for a ring oscillator circuit before etching the metal layers. **b**, Patterned Au electrode lines with ~2 μm width after etching and stripping the resist. The insets show magnified images. **c**, Au electrode lines (widths ~2 μm). **d**, Array of source/drain electrode pairs formed by e-jet printing of the resist layer, etching of metal and then stripping the resist. The inset shows an electrode pair separated by ~1 μm. **e**, AFM image and depth profile of a portion of this pair.

currents that are between ~1.5 and ~4.5 (inset of Fig. 6c), as expected owing to the population of metallic tubes in the arrays. Figure 6d (black circles) shows approximate device mobilities evaluated in the linear regime, calculated from the physical widths of source/drain electrodes ($W = 80\,\mu m$), a parallel-plate model for capacitance ($C$), and the transfer curves, according to $\mu_{dev} = (L/WCV_D) \cdot (\partial I_D/\partial V_G)$. These mobilities are between 7 and 42 $cm^2\,V^{-1}\,s^{-1}$ with $L$ in the range of 1–42 μm, and decrease with $L$ owing to the contact resistance[41–43]. The nature of electrostatic capacitance coupling of the gate to the SWNTs is important to the behaviour of these devices. Calculations of this gate capacitance are given in the Supplementary Information. This accurate capacitance model yields mobilities of 20–141 $cm^2\,V^{-1}\,s^{-1}$, as shown in Fig. 6d (red squares). We speculate that exposing the tubes to etchants for Cr/Au can induce defects, thereby resulting in lower mobilities than those reported previously with devices fabricated by other means[41]. The on/off ratios can be enhanced by an electrical breakdown process[41]. Transfer curves evaluated before and after this process are compared in Fig. 6e, for the case of a transistor with $L = 22\,\mu m$. The on/off ratio improves to >1,000 without substantial reduction in mobility (28 to 21 $cm^2\,V^{-1}\,s^{-1}$). Figure 6f shows full current–voltage characteristics before (inset) and after breakdown. Figure 6g shows an optical micrograph of a set of devices on a flexible sheet of polyimide, and Fig. 6h shows the normalized mobility and on/off ratio as a function of bending-induced strain[44] ($\varepsilon$). No significant change in the mobility or on/off ratio occurs for bending to radii of curvature ($R_C$) as small as 2 mm.

The advantages of this high-resolution form of e-jet printing over conventional ink-jet printing lie mainly in the high levels of resolution that can be obtained. We expect, in fact, that further reductions in the nozzle dimensions will enable resolution even deeper into the nanoscale. Achieving resolution at this level represents a topic of current work. The speeds for printing, using the particular systems described here, are relatively slow, although multiple-nozzle implementations, conceptually similar to those used in conventional ink-jet print heads, can reduce the printing duration. Key findings from analysis of throughput with conventional ink-jet printing systems also apply to the e-jet approach[45]. A main disadvantage of the e-jet approach is that the printed droplets have substantial charge that might lead to unwanted consequences in resolution and in device performance, particularly when used with electrically important layers such as gate dielectrics and semiconductor films. The

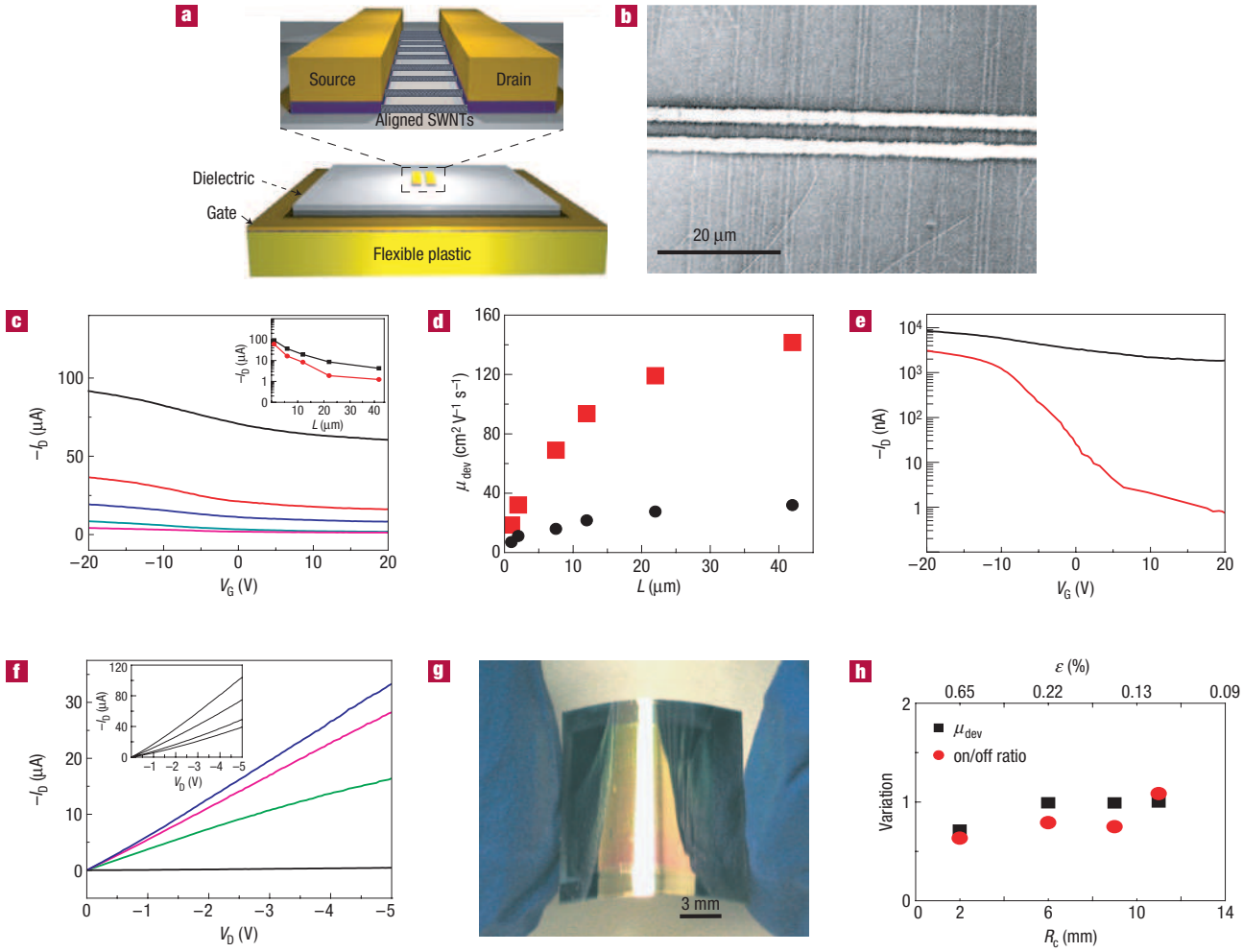


**Figure 6 Fabrication of perfectly aligned SWNT-TFTs on a plastic substrate with e-jet printing for the critical features, that is, the source and drain electrodes.** **a**, Schematic diagram of the transistor layout, where the source/drain electrodes are patterned by e-jet printing. **b**, SEM image of the aligned SWNTs connected by e-jet-printed source/drain electrodes. The tube density is ~2.5 SWNTs/10 μm. **c**, Transfer curves measured from transistors with channel lengths, $L = 1$, 6, 12, 22 and 42 μm, from top to bottom, and channel widths, $W = 80$ μm at a source/drain voltage, $V_D = -0.5$ V. The inset shows on and off currents (black and red lines, respectively) as a function of $L$. **d**, Linear-regime device mobilities ($\mu_{dev}$) calculated from the parallel-plate (black circles) and rigorous (red squares) capacitance models, as a function of $L$. **e**, Transfer curves from a transistor with $L = 22$ μm before (black line) and after (red) an electrical breakdown process. This breakdown reduces the 'off' current to less than ~1 nA to yield an on/off ratio of ~1,000. **f**, Current–voltage characteristics recorded after the electrical breakdown process. The gate voltage varies between −20 and 10 V in steps of −10 V, from top to bottom. The inset shows the current–voltage curve before the breakdown with the same gate voltages for comparison. **g**, Photograph of an array of flexible SWNT-TFTs. **h**, Variation of the normalized mobility (black squares) and on/off ratio (red circles) of a SWNT-TFT as a function of bending-induced strain ($\varepsilon$) and the radii to curvature ($R_c$).

effects of this charge might be minimized by using high-frequency alternating driving voltages for the e-jet process. These and other process improvements, together with exploration of applications in biotechnology and other areas, represent promising areas for future work.

## METHODS

### PREPARATION OF NOZZLES

Au/Pd (70 nm thickness) and Au (50 nm) layers were coated onto glass pipettes with tip internal diameters of between 0.3 and 30 μm (World Precision Instruments) using a sputter coater (Denton, Desk II TSC). Dipping the tip of the metal-coated pipette into 1H, 1H, 2H, 2H-perfluorodecane-1-thiol (Fluorous Technologies) solution (0.1 wt% in dimethylformamide) for 10 min formed a hydrophobic self-assembled layer on the gold surface of the nozzle tip. The capillary was connected to a syringe pump (Harvard Apparatus, Picoplus) or a pneumatic pressure actuator through a polyethylene tube.

### SYNTHESIS OF FUNCTIONAL INKS

PEDOT/PSS ink: PEDOT/PSS (Baytron P, H.C. Starck) was diluted with $H_2O$ (50 wt%), and then mixed with polyethyleneglycol methyl ether (Aldrich, 15 wt%) to reduce the surface tension (to lower the voltage needed to initiate printing) and the drying rate at the nozzle.

Single-crystal Si rods: Patterning the top Si layer (thickness: ~3 μm) of a silicon-on-insulator wafer by reactive ion etching, and then etching the underlying $SiO_2$ with an aqueous etchant of HF (49%)[38] with 0.1% of a surfactant (Triton X-100, Aldrich) formed the rods. These rods were suspended

in $H_2O$ and then filtered through filter paper (pore size: 300 nm). The rods were then suspended in 1-octanol. After printing this ink, the surfactant residue was thermally removed by heating to 400 °C in air for 5 h.

Ferritin: First, ferritin (Sigma) was diluted in $H_2O$ with a volume ratio of 1(ferritin):200($H_2O$). Then 1 wt% of a surfactant (Triton X-100) was added to this solution to reduce the surface tension (to lower the voltage needed to initiate printing). The surfactant residue was removed at 500 °C before CVD growth of SWNTs.

SWNT solution: Single-walled carbon nanotubes produced by the electric arc method (P2-SWNT, Carbon Solution) were suspended in aqueous octyl-phenoxy-polyethoxyethanol (Triton X-405, 2 wt%). The concentration was ~6.9 mg $l^{-1}$.

### PREPARATION OF SUBSTRATES

Si wafers with 300-nm-thick layers of thermal $SiO_2$ (Process Specialties) were used as substrates. The underlying Si was electrically grounded during printing. A glass slide (thickness: ~100 μm) was used for fluorescence optical micrography (Fig. 3c), and an ST-cut quartz wafer was used after annealing at 900 °C for guided growth of SWNTs (Fig. 3e). Here, the glass/quartz substrates were placed on an electrically grounded metal plate during printing. For printing of complex images (Figs 3f, 4a,b), the Si wafers were exposed to perfluorosilane vapour before e-jet printing to produce a hydrophobic self-assembled monolayer.

Received 23 February 2007; accepted 21 June 2007; published 5 August 2007.

## References


1. Forrest, S. R. The path to ubiquitous and low-cost organic electronic applications on plastics. *Nature* **428**, 911–918 (2004).
2. Gans, B. J., Duineveld, P. C. & Schubert, U. S. Inkjet printing of polymers: State of the art and future development. *Adv. Mater.* **16**, 203–213 (2004).
3. Parashkov, R., Becker, E., Riedl, T., Johannes, H. & Kowalsky, W. Large area electronics using printing method. *Proc. IEEE* **93**, 1321–1329 (2005).
4. Chang, P. C. *et al.* Film morphology and thin film transistor performance of solution-processed oligothiophenes. *Chem. Mater.* **16**, 4783–4789 (2004).
5. Sirringhaus, H. *et al.* High-resolution inkjet printing of all-polymer transistor circuits. *Science* **290**, 2123–2126 (2000).
6. Shimoda, T. *et al.* Solution-processed silicon films and transistors. *Nature* **440**, 783–786 (2006).
7. Burns, S. E., Cain, P., Mills, J., Wang, J. & Sirringhaus, H. Inkjet printing of polymer thin-film transistor circuits. *Mater. Res. Soc. Bull.* **28**, 829–834 (2003).
8. Wong, W. S., Ready, S. E., Lu, J. P. & Street, R. A. Hydrogenated amorphous silicon thin-film transistor arrays fabricated by digital lithography. *IEEE Electron Device Lett.* **24**, 577–579 (2003).
9. Szczech, J. B., Megaridis, C. M., Gamota, D. R. & Zhang, J. Fine-line conductor manufacturing using drop-on-demand PZT printing technology. *IEEE Trans. Electron. Packag. Manufactur.* **25**, 26–33 (2002).
10. Shimoda, T., Morii, K., Seki, S. & Kiguchi, H. Inkjet printing of light-emitting polymer displays. *Mater. Res. Soc. Bull.* **28**, 821–827 (2003).
11. Chang, S. C. *et al.* Multicolor organic light-emitting diodes processed by hybrid inkjet printing. *Adv. Mater.* **11**, 734–737 (1999).
12. Hebner, T. R. & Sturm, J. C. Local tuning of organic light-emitting diode color by dye droplet application. *Appl. Phys. Lett.* **73**, 1775–1777 (1998).
13. Lemmo, A. V., Rose, D. J. & Tisone, T. C. Inkjet dispensing technology: Application in drug discovery. *Curr. Opin. Biotechnol.* **9**, 615–617 (1998).
14. Heller, M. J. DNA microarray technology: Devices, systems, and applications. *Annu. Rev. Biomed. Eng.* **4**, 129–153 (2002).
15. Nallani, A., Chen, T., Lee, J. B., Hayes, D. & Wallace, D. Wafer level optoelectronic device packaging using MEMS. *Proc. SPIE: Smart Sensors Actuators MEMS II* **5836**, 116–127 (2005).
16. Bietsch, A., Zhang, J., Hegner, M., Lang, H. P. & Gerber, C. Rapid functionalization of cantilever array sensors by inkjet printing. *Nanotechnology* **15**, 873–880 (2004).
17. Hiller, J., Mendelsohn, J. D. & Rubner, M. F. Reversibly erasable nanoporous anti-reflection coatings from polyelectrolyte multilayers. *Nature Mater.* **1**, 59–63 (2002).
18. Ling, M. M. & Bao, Z. Thin film deposition, patterning, and printing in organic thin film transistors. *Chem. Mater.* **16**, 4824–4840 (2004).
19. Calvert, P. Inkjet printing for materials and devices. *Chem. Mater.* **13**, 3299–3305 (2001).
20. Sanaur, S., Whalley, A., Alameddine, B., Carnes, M. & Nuckolls, C. Jet-printed electrodes and semiconducting oligomers for elaboration of organic thin-film transistors. *Org. Electron.* **7**, 423–427 (2006).
21. Cheng, K. *et al.* Inkjet printing, self-assembled polyelectrolytes, and electroless plating: Low cost fabrication of circuits on a flexible substrate at room temperature. *Macromol. Rapid Commun.* **26**, 247–264 (2005).
22. Creagh, L. T. & McDonald, M. Design and performance of inkjet printheads for non graphic arts applications. *Mater. Res. Soc. Bull.* **28**, 807 (2003).
23. Wang, J. Z., Gu, J., Zenhausern, F. & Sirringhaus, H. Low-cost fabrication of submicron all polymer field effect transistors. *Appl. Phys. Lett.* **88**, 133502 (2006).
24. Stutzmann, N., Friend, R. H. & Sirringhaus, H. Self-aligned, vertical channel, polymer field effect transistors. *Science* **299**, 1881–1885 (2003).
25. Sele, C. W., Werne, T., Friend, R. H. & Sirringhaus, H. Lithography-free, self-aligned inkjet printing with sub-hundred nanometer resolution. *Adv. Mater.* **17**, 997–1001 (2005).
26. Mills, R. S. *Recent Progress in Ink Jet Technologies II* 286–290 (Society for Imaging Science and Technology, Washington, 1999).
27. Nakao, H., Murakami, T., Hirahara, S., Nagato, H. & Nomura, Y. *IS&Ts NIP15: 1999 International Conference on Digital Printing Technologies* 319–322 (Society for Imaging Science and Technology, Washington, 1999).
28. Choi, D. H. & Lee, F. C. *Proc. of IS&T's Ninth International Congress on Advances in Non-Impact Printing Technologies. October 4–8, Yokohama, Japan* (Society for Imaging Science and Technology, Washington, 1993).
29. Kawamoto, H., Umezu, S. & Koizumi, R. Fundamental investigation on electrostatic ink jet phenomena in pin-to-plate discharge system. *J. Imaging Sci. Technol.* **49**, 19–27 (2005).
30. Taylor, G. Disintegration of water droplets in an electric field. *Proc. R. Soc. Lond. A* **280**, 383–397 (1964).
31. Jayasinghe, S. N. & Edirisinghe, M. J. Electric-field driven jetting from dielectric liquids. *Appl. Phys. Lett.* **85**, 4243 (2004).
32. Marginean, I., Parvin, L., Heffernan, L. & Vertes, A. Flexing the electrified meniscus: The birth of a jet in electrosprays. *Anal. Chem.* **76**, 4202–4207 (2004).
33. Chen, C. H., Saville, D. A. & Aksay, I. A. Scaling law for pulsed electrohydrodynamic drop formation. *Appl. Phys. Lett.* **89**, 124103 (2006).
34. Hayati, I., Bailey, A. I. & Tadros, T. F. Investigations into mechanisms of electrohydrodynamic spraying of liquids. *J. Colloid Interface Sci.* **117**, 205–221 (1987).
35. Wickware, P. & Smaglik, P. Mass spectroscopy: Mix and match. *Nature* **413**, 869 (2001).
36. Salata, O. V. Tools of nanotechnology: Electrospray. *Curr. Nanosci.* **1**, 25–33 (2005).
37. Smith, A. *et al.* Observation of strong direct-like oscillator strength in the photoluminescence of Si nanoparticles. *Phys. Rev. B* **72**, 205307 (2005).
38. Menard, E., Lee, K. J., Khang, D. Y., Nuzzo, R. G. & Rogers, J. A. A printable form of silicon for high performance thin film transistors on plastic substrates. *Appl. Phys. Lett.* **84**, 5398 (2004).
39. Kocabas, C., Shim, M. & Rogers, J. A. Spatially selective guided growth of high-coverage arrays and random networks of single-walled carbon nanotubes and their integration into electronic devices. *J. Am. Chem. Soc.* **128**, 4540–4541 (2006).
40. Park, J. U. *et al.* In situ deposition and patterning of single walled carbon nanotubes by laminar flow and controlled flocculation in microfluidic channels. *Angew. Chem. Int. Edn* **45**, 581–585 (2006).
41. Kang, S. J. *et al.* High performance electronics using dense, perfectly aligned arrays of single walled carbon nanotubes. *Nature Nanotechnol.* **2**, 230–236 (2007).
42. Chen, Z., Appenzeller, J., Knoch, J., Lin, Y. M. & Avouris, P. The role of metal-nanotube contact in the performance of carbon nanotube field effect transistors. *Nano Lett.* **5**, 1497–1502 (2005).
43. Kim, W. *et al.* Electrical contacts to carbon nanotubes down to 1 nm in diameter. *Appl. Phys. Lett.* **87**, 173101 (2005).
44. Lee, K. J. *et al.* A printable form of single-crystalline gallium nitride for flexible optoelectronic systems. *Small* **1**, 1164–1168 (2005).
45. Sheats, J. R. Manufacturing and commercialization issues in organic electronics. *J. Mater. Res.* **19**, 1974–1989 (2004).


## Acknowledgements

The authors thank L. Jang and M. Nayfeh for supplying Si nanoparticle solutions, R. Shepherd and J. Lewis for the use of their high-speed camera, and R. Lin for assistance with setting initial experimental conditions. In addition, the authors acknowledge the Center for Nanoscale Chemical Electrical Mechanical Manufacturing Systems in the University of Illinois, which is funded by the National Science Foundation under grant DMI-0328162, and the Center for Microanalysis of Materials in University of Illinois, which is partially supported by the US Department of Energy under grant DEFG02-91-ER45439.
Correspondence and requests for materials should be addressed to J.A.R.
Supplementary Information accompanies this paper on www.nature.com/naturematerials.

## Author contributions

J.-U.P. and J.A.R. designed the experiments and wrote the paper. J.-U.P. carried out the nozzle fabrication, ink design, printing and characterization. S.J.K. and J.-U.P. contributed to device fabrication. K.B., K.A., D.K.M., A.G.A. and P.M.F. designed the printing machine and contributed to project planning. J.G.G. was responsible for hydrodynamics analysis and project planning. C.Y.L. and M.S.S. synthesized SWNT solutions. M.H. developed the software algorithm and measured contact angles.

## Competing financial interests

The authors declare no competing financial interests.